Micro-thermography for imaging ice crystal growth and nucleation inside non-transparent materials

Martin Zalazar[1,a)], Fredy Zypman[2], and Ran Drori[1,b)]

[1]Department of Chemistry and Biochemistry, Stern College, New York, NY
[2] Department of Physics, Yeshiva College, New York, NY

a) Also at: Instituto de Investigación y Desarrollo en Bioingeniería y Bioinformática (CONICET-UNER) and Facultad de Ingeniería, Universidad Nacional de Entre Ríos, Ruta Prov. 11 (Km 10), (3101) Oro Verde, Entre Ríos, Argentina.

b) Author to whom correspondence should be addressed: rdrori@yu.edu

Abstract

Ice crystal growth and nucleation rate measurements are usually done using light microscopy in liquid and transparent samples. Yet, the understanding of important practical problems depends on monitoring ice growth inside solid materials. For example, how rapid ice growth leads to structural damage of food, or how the final structure of cementitious materials is affected by ice during curing. Imaging crystal growth inside solid materials cannot be done with visible light and is intrinsically more challenging than visible light imaging. Thermography is a technique that uses thermal (Infra-red) cameras to monitor temperature changes in a material, and it has been used to provide qualitative description of ice propagation with a low spatial resolution. Here, we describe a method that uses a novel micro-thermography system to image ice nucleation and growth inside non-transparent samples. This method relies on two major components: a cold stage with accurate temperature control (±0.001 ºC) and a thermal camera with high spatial and temperature resolution. Our experiments include imaging of ice formation and growth in pure water first, and inside plant leaves used as a model for a non-transparent material. Ice growth rate of 2.2 mm/s was measured inside a plant leaf at -12 ºC and ice nucleation in single plant cells was observed as a hot spot having a diameter of 160 μm. The results presented here provide experimental proof that high-quality imaging of ice growth is achievable, thus paving the way to quantitative measurements of ice growth kinetics and ice nucleation in solid materials.

Significance Statement

Current techniques to study ice growth are limited to liquid and transparent samples. Using thermal imaging and a temperature-controlled stage, we describe a new micro-thermography technique designed to image ice formation and growth inside various materials with an improved spatial and temperature resolution. The measurement of a temperature profile across ice crystals to quantify the exchange of heat between the ice and the liquid water, represents a novel approach for thermal imaging as was demonstrated for nucleation events in liquid samples and plants.

INTRODUCTION

Ice nucleation and recrystallization plays a central role in our daily lives and understanding these processes will have great implications. Imaging ice formation and freezing of non-transparent samples is a challenge, as most methods use visible light-based imaging. Developing a new method that would allow for imaging of ice growth in non-transparent samples is beneficial in many fields such as frozen food[1–3], cement-based materials[4], and plant health[5–7]. When the temperature of the sample is lowered below the equilibrium melting point (~0 °C), the water molecules become supercooled, i.e., exist as liquid below the melting point. As the temperature continues to decrease, a small ice nucleus is formed, and rapid ice growth occurs. This process leads to the deterioration of food quality, as solutes start to concentrate in the food, ice causes structural damage to the food and proteins start to aggregate. Upon

thawing, the food product may lose its structural integrity and drip loss occurs[8]. In a similar way, ice growth in cementitious materials might lead to weakening of the final structure[4]. Understanding the process of ice nucleation and growth and obtaining quantitative measurements such as nucleation and growth rates in non-transparent samples would be a major advantage in the effort to limit damages caused by ice. Furthermore, understanding the mechanism by which biological ice nucleators[9–12] such as ice-nucleation proteins (INPs) dramatically increase the nucleation temperature will be beneficial. These INPs are produced by bacteria such as *Pseudomonas syringae* and are secreted from the bacterial cell to puncture the plant epidermis using ice nucleation[7,13].

One way to image ice growing inside non-transparent samples is thermography, a technique that uses thermal (Infra-red) cameras to monitor temperature changes in the sample. As ice growth and melting releases or absorbs heat, thermal cameras can capture these phase changes inside various types of samples. Indeed, thermographic methods were successfully implemented to characterize ice nucleation and growth in frozen food[14–16] and plant health[5–7]. However, these studies provided a mostly qualitative description of ice propagation and nucleation, and the spatial resolution used in these studies (a few mm) is limited.

The aim of this paper is to present and describe the development of a micro-thermography system that specializes in capturing ice nucleation and growth in non-transparent samples. Using a cold stage with accurate temperature control (±0.001 ºC)[17] coupled to a high-resolution thermal camera, we explore ice nucleation and growth processes in pure water and inside plant leaves, chosen as a model sample.. The method described here uses temperature differences in the sample to analyze crystallization and melting events, which is achieved by relying on the release of heat from ice crystallization. This report provides clear evidence that micro-thermography effectively captures heat signatures coming from ice growth and melting inside various materials at a single-cell resolution.

MATERIALS AND METHODS

Temperature control system and thermal imaging

A temperature controller was used to control and power a thermoelectric Peltier module, which needs to be controlled precisely and quickly providing sharp and prompt control of the temperature. Proportional-Integral-Derivative (PID) control is the most common control algorithm and consists of three basic coefficients: proportional, integral, and derivative which are varied to get optimal response. Traditional PID controllers are linear and require the development of an optimal tuning method for the PID controller[18]. These types of controllers need to work with negative temperature coefficient (NTC) thermistors as their resistance sensitivity is a critical parameter of the system.

The 585-05-12 Tek Pack Temperature Controller (Arroyo Instruments, San Luis Obispo, CA) was used here and the Ziegler-Nicholes tuning method was applied since it is the most well-known and reliable heuristic method for PID tuning. The PID Tuner app from MATLAB™ for plant estimation was used, as it automatically tunes the gains of a PID controller to identify a linear plant model from the measured response data. This control is a closed-loop control scheme, which means feedback is employed for controlling the temperature on the sensor module. For this purpose, an NTC thermistor (TDK B57540G1) was incorporated

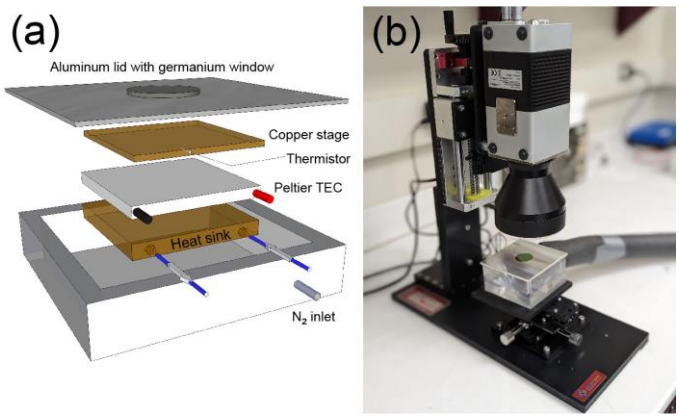

Fig. 1. Thermography and thermal control system. a) Peltier cell-based cold stage surrounded by a copper plate on top and a heat sink at the bottom. The N_2 inlet and the Al lid help to avoid condensation into the system. b) Infra-red camera positioning setup. The moving stage gives precision in the location of the visualized sample.

for temperature sensing due to its small dimensions, fast response time and precision, also being heat-resistive and highly stable.

A cold stage was constructed in our laboratory by fabricating an acrylic box using a CNC machine. The box housed a thermoelectric Peltier module and a water block, which functions as a heat sink (Custom Thermoelectric, Ocean City, Maryland). A copper plate was placed on the Peltier module and thermal grease was applied on both surfaces. A 10 kOhm thermistor was inserted into a hole drilled into the narrow face of the copper plate (see Fig. 1a). An aluminum lid (Custom Thermoelectric, Ocean City, Maryland) with a germanium window (Edmund Optics, Barrington, NJ) was used to prevent condensation on the window. Thermal control has a -40 °C to 80 °C nominal working range and bidirectional control heating and cooling. The thermal camera (VarioCAM® HD head 800 with Micro-scanning upgrade, InfraTec GmbH, Germany) was mounted on an XYZ stage (Ekrub Nano, San Ramon, CA), having a spatial resolution of 8 µm and temperature resolution of 0.03 ºC (Fig. 1b). The temperature obtained by the camera was calibrated for various samples (water, ice and leaves) to match the temperature of the cold stage. This calibration was performed by setting the sample on the cold stage, and while maintaining a constant temperature for ~30 s, an image was obtained for each temperature (ranging 10 to -20 °C). Then, the temperature obtained by the thermal camera was corrected by a formula to achieve the same temperature as the cold stage (see SI for further information).

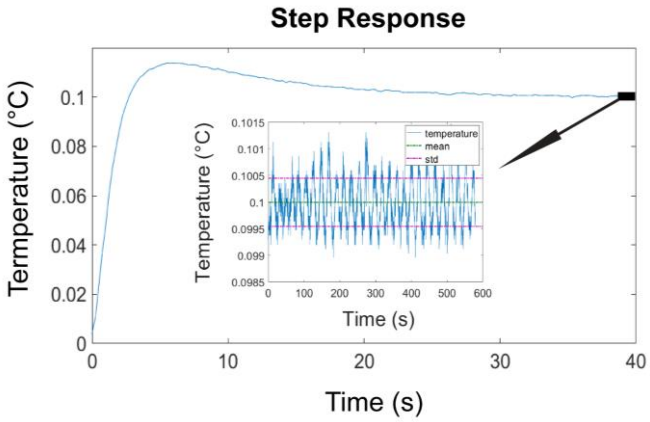

Fig. 2. The step-response characteristics of the temperature system (thermoelectric module and controller) is shown; rise time (time it takes to go from 10% to 90% of the final value), settling time (time required to settle within 2% of the final value), and overshoot were calculated (1.84 s, 27.35 s, and 13.98 % respectively). Stability and resolution of the system are depicted in the inset by using descriptive statistics (mean and standard deviation).

Temperature control system performance

The obtained temperature stability and resolution using the cold stage system are crucial for controlling the growth and melting of micron-sized ice crystals. The step-response characteristics of the system were obtained (Fig. 2). Temperature step from 0 °C to +0.1°C was used to excite the system and the behavior of the temperature over time was recorded, having a rise time of 1.84 s, a settling time of 27.35 s, and an overshoot of 13.98%.

Experiments with pure water and leaves

The experiments presented here were preformed using the following samples:

A. Pure water
   - Water in oil (3 µL droplet injected to oil)
   - Splat sample (5 µL droplet dropped from 1.5 m on a cold surface)

B. Biological sample
   - Dwarf lilyturf fresh leaves (1 mm thickness, 6 mm width).

The experiments with pure water included a few types of sample preparations. For ice nucleation experiments, a small Type B immersion oil droplet (Cargille Laboratories, Cedar Grove, NJ) was deposited on a sapphire disc (25.4 mm in diameter, 0.3 mm thick) (Ted Pella, Redding, CA), which was placed on the cold stage. A sample of 3 µL was injected into the oil droplet to avoid evaporation of the water during the experiment. To obtain thin samples for imaging growth/melting of ice crystals, we used the splat assay[19], in which a 5 µL droplet of pure water was released from a pipette held at 1.5 m

above the cold stage. The droplet went through a long tube (a Dyson cordless vacuum tube) to make sure it lands on the cold stage. The temperature of the cold stage was set to -30 °C and the droplet froze immediately after hitting the sapphire disc, creating a thin layer of ice. Experiments with plant leaves were obtained by placing fresh plant leaves of Dwarf lilyturf on the sapphire disc. In all experiments, nitrogen gas was flowed into the acrylic box that housed the cold stage to prevent condensation. The ice growth rate was measured in leaves by video analysis of the advancing ice front captured by the thermal camera at a rate of 2.5 - 7 frame/s.

EXPERIMENTAL RESULTS

Ice in pure water

The first experiments with the thermal camera included ice nucleation, since the heat generated in the nucleation event should be significant enough for small volumes (3 µL). Using a pippete, 3 µL of pure water were injected into the oil droplet to avoid evaporation of the water. Temperature of the cold stage was decreased from room temperature to -25 °C at a rate of 0.5 °C/s while capturing the process using the thermal camera.. At -20 °C, a clear heat signature was observed (Fig. 3a, t = 0.26 s), which signifies the nucleation event followed by the dissipation of heat away from the newly formed ice (Fig. 3, t = 4.01s - 6.68 s). The local temperature at the moment of nucleation increased by 20°C, which is presented in Fig. 3b using 3D plots generated by the thermal camera software (IRBIS® 3). After obtaining information on the heat release and its dissipation during ice nucleation, the next step included imaging ice crystals in pure water and characterizing their heat signature during freezing and melting. Imaging ice crystals using thermography is challenging since the signal from the ice is obtained by the release or absorbance of heat, which happens when the ice grows or melts. Thus, when the ice crystals are static, the camera is not able to distinguish between the ice and the surrounding water. To obtain a clear signal of phase changes, ice crystals were first grown in pure water.

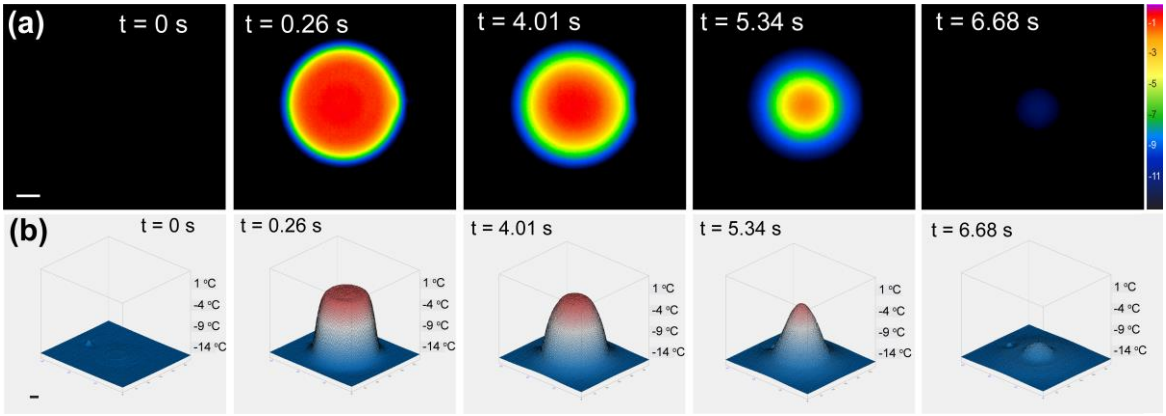

Fig. 3. Ice nucleation in pure water as imaged by the thermal camera provided insights into the rate of heat release and dissipation after the nucleation event. The water sample (3 µL) was injected into a droplet of oil to prevent evaporation of the sample. a) time evolution of the nucleation event at ~-17 °C , and b) 3D plots generated by the camera software. Scale bar = 500 µm.

Controlling ice growth/melting in a thick sample (3 µL in oil) is very challenging as temperature gradients have a stronger effect compared to thin samples. Also, a thick sample includes multiple layers of ice, which might generate overlapping thermal signals. To obtain a thin layer of ice on the sapphire disc, the splat assay was used[19]. The sapphire disk was treated with plasma (Harrick Plasma, Ithaca, NY) to obtain a hydrophilic surface. Next, a 5 µL droplet of pure water was dropped from a pipette held 1.5 m above the sapphire disc, which was placed on the cold stage while the temperature was set to -30 °C. Then, the temperature was increased to ~-1 °C, and was then slowly increased to reach 0 °C. When the temperature approached 0 °C, the ice layer started to melt, and the thermal camera captured this melting event (Fig. 4a) as ice absorbed the heat around it. The temperature was then decreased to -1.3 °C, which caused the ice to stop melting or growing (Fig. 4b), followed by rapid growth and the release of heat from the ice to the surrounding liquid water (Fig. 4c). To quantify the exchange of heat between

the ice and the liquid water, a temperature profile across the ice crystal was created (Fig. 4, right hand side). When the ice was melting (Fig 4a), the temperature profile exhibits a well, which is attributed to the heat absorbed by the ice crystal during melting. After the temperature was decreased, the ice stopped melting or growing, and a flat temperature profile was observed (Fig. 4b). As the temperature continued to decrease and the ice crystal grew, a peak was observed in the temperature profile, signifying the release of heat (Fig. 4c). Adding the temperature profiles of all frames of this sequence into one plot provides an interesting insight (Fig. 5). In the spatial range between 1000 and 1700 µm (corresponding to the ice crystal presented in Fig. 4), the temperature is constant within the experimental error of 0.06 ºC, while the temperature outside this range was decreased by 1.35 °C. Thus, the temperature at the region 1000-1700 µm is unchanged during the temperature decrease because of phase change, as the ice grows. In addition, an accurate melting point of the ice crystals was extracted from the 1000-1700 µm region (black line, Fig. 5) and was found to be -0.59 ± 0.06 ºC.

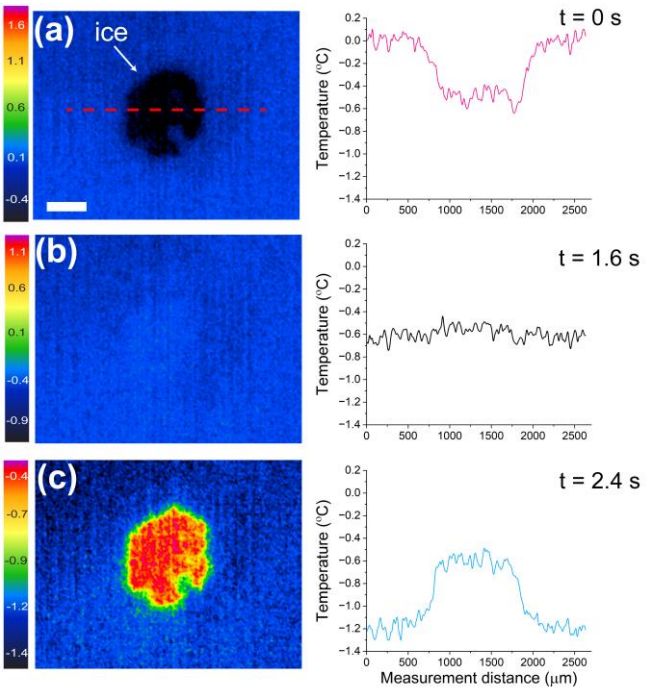

Fig. 4. Thermal imaging of ice melting and growing in a pure water droplet. a) Ice melting when temperature is slightly above the melting point, and showing a well in the temperature profile. b) After the temperature of the cold stage was lowered, the crystal was no longer melting, which is indicated by the flat temperature profile. c) As the temperature was lowered furhter, heat release from the ice crystal growth was observed, and a peak in the temperature profile is presented (phase change). Scale bar = 400 µm.

Ice growth inside biological samples

The experiments with ice in pure water described above provided a good starting point to image ice in non-transparent samples, which included leaves of Dwarf lilyturf, available in New York City. These leaves are ~1 mm thick and ~6 mm wide, which was a good fit for the field of view of the thermal camera. The leaves were cut to ~1-2 cm long pieces and were placed on the sapphire disc that was resting on the cold stage. The procedure was carried out by setting the temperature to -25 °C to ensure a fully frozen leaf while recording the process using the thermal camera. When the temperature reached

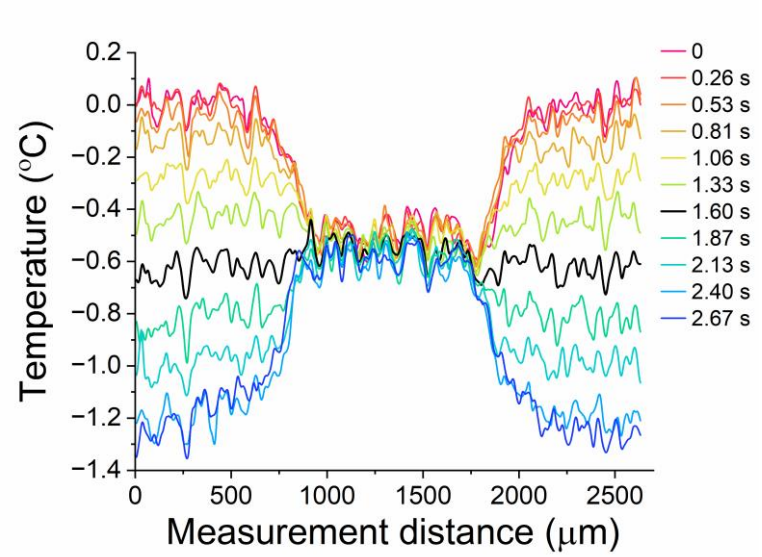

Fig. 5. Temperature profile of ice melting and growing in a pure water droplet (as shown in Fig. 4). The melting point was extracted from the 900-1700 µm region where the temperature remains constant, while the temperature in other regions decreasd by 1.3 °C. The black line at t = 1.60 indicates the melting point of the sample (-0.59 ± 0.06 ºC).

~-5 °C, small and short-lived flashes of heat started to randomly appear in the sample. These flashes of heat indicate stochastic ice nucleation events, which were observed throughout the sample in random order. Such a hot spot is presented in Fig. 6 during a short window of time (0.27 s) and having a diameter of 160 µm. The typical size of a plant cell ranges between 10 and 100 µm[20], thus this nucleation event might be limited to one or two cells. This type of cell-by-cell ice nucleation in plant leaves was also observed in a previous study that used thermography[5]. After the entire leaf froze, the temperature of the cold stage was raised to 10 °C and all the ice melted. The temperature was lowered again to -25 °C to repeat the freezing event. This time, a nucleation event was observed, but the ice progressed inside the leaf continuously, which is contrary to the cell-by-cell nucleation observed on the first freezing experiment. The continuous progress of ice inside the leaf is presented in Fig. 7a and the ice growth rate was analyzed by registering the ice growth frame by frame. The growth rate of 2.2 mm/s was measured along the fastest growing direction of the crystal (the *a*-direction, perpendicular to the prism plane) at -12 °C. The advancing ice front starting from a small ice nucleus at the bottom of the leaf can be seen while the ice grew until the leaf was completely frozen (Fig. 7a). To image ice melting, the temperature was increased to ~+2 °C and two cold spots were observed. The size of these cold spots decreased as the temperature of the cold stage increased (Fig. 7b), suggesting that these are ice crystals. These proof-of-concept experiments provide strong evidence for the prospects of high-quality imaging of ice growth inside non-transparent samples, which will lead to quantitative measurements of ice growth velocity and ice nucleation in biological samples.

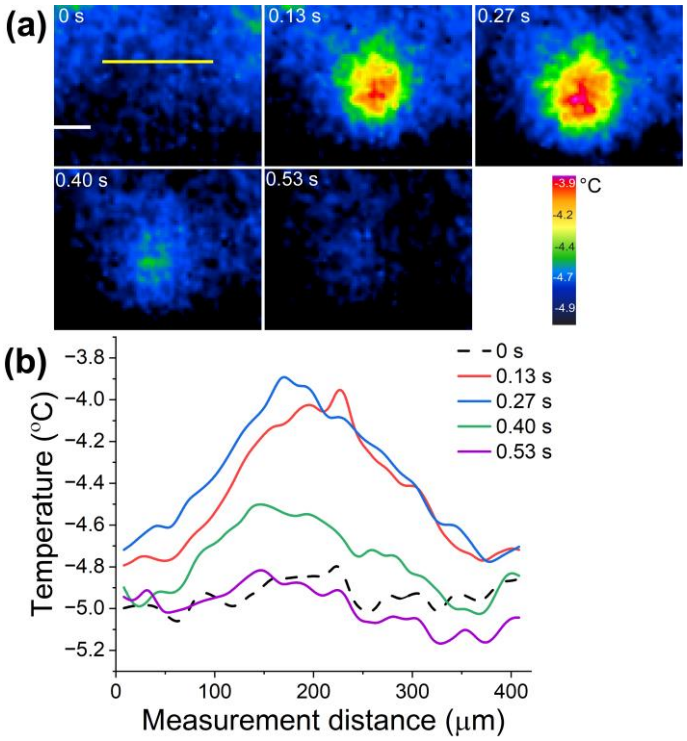

Fig. 6. (a) Time evolution of ice nucleation in single plant cells was observed when the temperature was lowered to ~-15 °C. An increase of 1.2 °C was observed, which signifies ice nucleation in one or two cells in the leaf. Scale bar = 100 µm. b) Temperature measurement across the nucleation site (yellow line in a) provides quantitative information on the heat increase during ice nucleation inside the cells. This sequence is presented as Multimedia view S1.

DISCUSSION

Micro-thermography is a powerful tool capable of imaging and quantifying temperature changes in small samples and providing high-resolution temperature distribution in various samples[21]. Coupling a high-resolution thermal camera to a highly precise cold stage provides an additional benefit of imaging ice growth in various non-transparent samples. Our results show that accurate measurements of ice growth and nucleation kinetics in various materials can be obtained. The used technique of pure water injected into oil droplets to avoid water evaporation is a reliable option when using thermal cameras, where the main challenge is finding materials that are transparent in the IR range to be used as sample covers. However, using a thin Germanium or CaF_2 window (1 mm thick) as a cover by placing it on top of the water droplet and creating a sandwiched sample[22], presented another challenge. The heat released by the ice nucleation event was absorbed by both the bottom of the sample (sapphire disc) and the cover (the Germanium window), and thus the camera was not able to capture the signal coming from the nucleation of ice. The splat technique was proved as an excellent solution as it provided a thin sample of an ice wafer, having a good thermal signal visualization. The observed heat signatures of ice

growth/melting inside a sample, indicate that these events can be captured using a thermal camera, as was demonstrated for nucleation events in liquid samples[23] and plants[5–7]. Ice nucleation of a water droplet (3 µL) inside oil has generated much more heat compared to ice growth at higher temperatures, which is an expected result, as the ice crystallizes much faster right after nucleation at these low temperatures (-20 ºC). The melting point of ice was identified by measuring the temperature of the ice crystal during growth and was found to be -0.59 ± 0.06 ºC. Using thermography, Castillo *et al.* found that the temperature of the progressing ice in a water droplet during nucleation is close to the melting point of ice (0 ºC)[24]. Indeed, in our nucleation experiments, the temperature has increased after ice nucleation close to the melting point of the sample (-0.9 ºC for pure water and -3.9 ºC for the leaves). In addition, the rate of heat dissipation after ice nucleation was faster at the periphery of the water droplet, thereby creating a cone shaped profile, which is different than the temperature profile obtained by Castillo *et al.*[24]. However, in this work, the water droplet was injected into oil, while Castillo *et al.* deposited the water droplet onto the cold-stage[24].

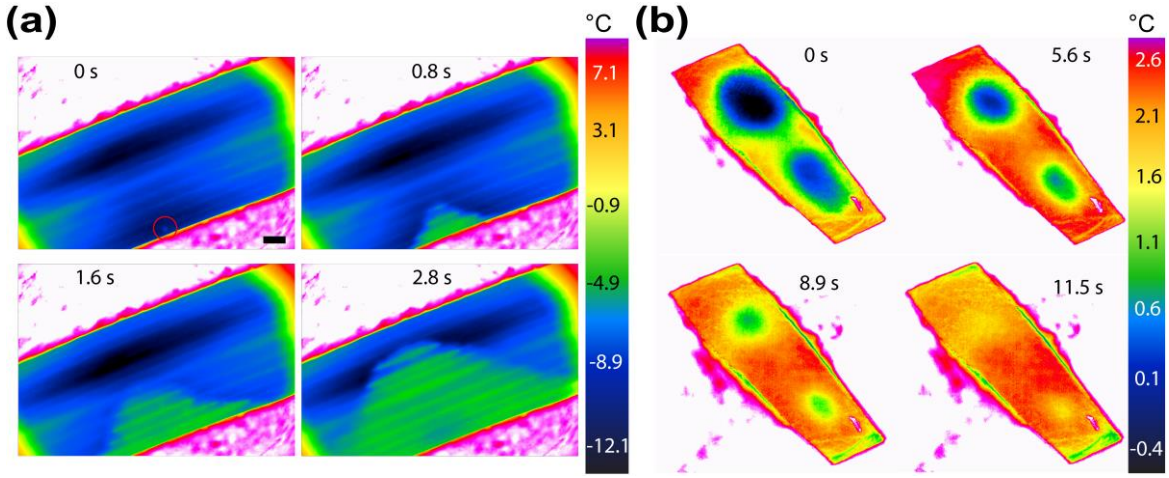

Fig. 7. Ice growth and melting inside a leaf. a) Advancing of ice front starting from a small ice crystal spot at the bottom of the leaf indicated by a red circle (See Multimedia view S2). Note that the advancing ice is warmer than the solution around it, as latent heat is released, indicating crystal growth. b) two frozen spots decreasing in size as the temperature of the cold stage is increased above the melting point. Note that the melting ice is colder compared to the unfrozen parts of the leaf around it, indicating ice melting. Scale bar in (a) = 1 mm. The temperature calibration in (a) and (b) was calculated for the sample (leaf) and not for the background of the leaf (sapphire disc).

Ice nucleation inside leaves provided an interesting biological phenomenon, where in the first nucleation event, isolated nucleation events were observed, while in the second freezing event of the leaf, the ice progressed through the leaf continuously. We hypothesize that in the first nucleation event, ice was confined to intracellular spaces, or in isolated intercellular areas. However, this nucleation event has probably destroyed some of the membranes and cell walls, which resulted in a rapid advance of the ice front in the second freezing event. These experiments have the potential to examine different biological samples (including food products) and test the damage caused by ice growth. The study of ice nucleation by INPs inside various materials using micro-thermography is exciting and should be explored. Previous experiments using thermography presented compelling results of the effect of INPs on ice nucleation inside plants[7].

CONCLUSIONS AND FUTURE WORK

This report demonstrates that the heat signature coming from ice growth and melting can be captured by micro-thermography at a single-cell resolution. This capability is a highly important milestone not only because of the ability of the system to capture nucleation and growth events inside non-transparent samples, but also since the user can quantify these parameters (temperature, shape, size, and time).

Thus, heat exchange between ice and liquid water can be quantified across a growing/melting ice crystal, and growth and nucleation rates inside the sample can be accurately measured. Encouraged by the results presented here, next steps will focus on developing new ways to improve the quality of frozen food products. The developed method will be applied to in-situ imaging of ice growth in frozen food, thus thriving to understand key insights into the freezing process of food samples.

SUPPLEMENTARY MATERIAL

A detailed description of the total thermal system (temperature control system and thermal imaging) calibration was done. Since the temperature measured by the thermal camera did not match the temperature measured in the cold stage, a series of temperature calibrations were conducted for various samples (liquid water, ice and leaves).

ACKNOWLEDGMENTS
The authors acknowledge the generous support from the United States Department of Agriculture, National Institute of Food and Agriculture (award number 2022-67018-36539).

AUTHOR DECLARATIONS
Conflict of Interest
The authors have no conflicts to disclose.

Author Contributions
RD conceptualized the research, MZ and RD preformed the experiments, wrote the paper, and analyzed the data. FZ developed the temperature calibration formula and data fitting.

DATA AVAILABILITY
The data that support the findings of this study are available from the corresponding author upon reasonable request.

References
[1] Z. Zhu, Q. Zhou, and D.W. Sun, Trends Food Sci. Technol. **90**, 13 (2019).
[2] L.D. Kaale and T.M. Eikevik, Trends Food Sci. Technol. **39**, 91 (2014).
[3] P.K. Kumar, B.A. Rasco, J. Tang, and S.S. Sablani, Food Eng. Rev. **12**, 421 (2020).
[4] S.D. Frazier, M.G. Matar, J. Osio-Norgaard, A.N. Aday, E.A. Delesky, and W. V. Srubar, Cell Reports Phys. Sci. **1**, (2020).
[5] D.P. Livingston, T.D. Tuong, J.P. Murphy, L. V. Gusta, I. Willick, and M.E. Wisniewski, Planta **247**, 791 (2018).
[6] B.A.A. Workmaster, J.P. Palta, and M. Wisniewski, J. Am. Soc. Hortic. Sci. **124**, 619 (1999).
[7] M. Wisniewski, G. Neuner, and L. V. Gusta, J. Vis. Exp. **2015**, 1 (2015).
[8] Paul Nesvadba, *Frozen Food Science and Technology* (Blackwell Publishing Ltd, 2008).
[9] L.R. Maki, E.L. Galyan, M.M. Chang-Chien, and D.R. Caldwell, Appl. Microbiol. **28**, 456 (1974).
[10] R. Schwidetzky, A.T. Kunert, M. Bonn, U. Pöschl, H. Ramløv, A.L. Devries, J. Fröhlich-Nowoisky, and K. Meister, J. Phys. Chem. B **124**, 4889 (2020).
[11] A. Hudait, N. Odendahl, Y. Qiu, F. Paesani, and V. Molinero, J. Am. Chem. Soc. **140**, 4905 (2018).
[12] M. Lukas, R. Schwidetzky, A.T. Kunert, E.H.G. Backus, U. Pöschl, J. Fröhlich-Nowoisky, M. Bonn, and K. Meister, J. Phys. Chem. Lett. **12**, 218 (2021).
[13] M. Lukas, R. Schwidetzky, R.J. Eufemio, M. Bonn, and K. Meister, J. Phys. Chem. B **126**, 1861 (2022).
[14] L. Cuibus, M. Castro-Giráldez, P.J. Fito, and A. Fabbri, Innov. Food Sci. Emerg. Technol. **24**, 80 (2014).

[15] B.J. Gonçalves, A.M.T. Lago, A.A. Machado, T.M. de O. Giarola, M.E.T. Prado, and J.V. de Resende, J. Food Eng. **221**, 77 (2018).
[16] D. Colucci, R. Maniaci, and D. Fissore, Int. J. Pharm. **566**, 488 (2019).
[17] R. Drori, M. Holmes-Cerfon, B. Kahr, R. V Kohn, and M.D. Ward, Proc Natl Acad Sci U S A **114**, 11627 (2017).
[18] M.M. Gani, M.S. Islam, and M.A. Ullah, SN Appl. Sci. **1**, 880 (2019).
[19] C.A. Knight, D. Wen, and R.A. Laursen, Cryobiology **32**, 23 (1995).
[20] K.H. Jensen and M.A. Zwieniecki, Phys. Rev. Lett. **110**, 1 (2013).
[21] S. Ferdinandus Arai, S. Takeoka, S. Ishiwata, M. Suzuki, and H. Sato, ACS Sensors **1**, 1222 (2016).
[22] R. Drori, C. Li, C. Hu, P. Raiteri, A.L. Rohl, M.D. Ward, and B. Kahr, J. Am. Chem. Soc. **138**, 13396 (2016).
[23] A.T. Kunert, M. Lamneck, F. Helleis, U. Pöschl, M.L. Pöhlker, and J. Fröhlich-Nowoisky, Atmos. Meas. Tech. **11**, 6327 (2018).
[24] J.E. Castillo, Y. Huang, Z. Pan, and J.A. Weibel, Int. J. Heat Mass Transf. **164**, 120608 (2021).